

can be varied from 400 cm^{-1} (50 fs) to 2400 cm^{-1} (8 fs) using slit and prism positions, and it provides 300–500 mW of power at 95 MHz repetition rate. To excite CARS of vibrational resonances in the characteristic region ($800\text{--}1800\text{ cm}^{-1}$), the laser was used at maximum bandwidth with a spectrum shown in the inset of Fig. 1. To provide a background free detection of the CARS signal in the range of 630–700 nm, the short wavelength tail of the laser was cut by a Schott RG9 filter of 6 mm thickness. The laser is split into Pump and Stokes pulses by a dichroic mirror (Chroma 770DCXRU, *s*-polarization). To compensate the different group-velocity dispersion (GVD) of glass for the two pulses, the Stokes propagates through a thickness L_1 of SF57 glass before it is recombined with the Pump with an adjustable delay t_0 in a second dichroic mirror of equal type. Both pulses then propagate through a thickness $L_2=2\text{ cm}$ of SF57 and enter the microscope setup described in Ref. 12. The resulting Pump and Stokes spectra are centered around 750 and 850 nm, respectively, as shown in the inset of Fig. 1. The total power transmission of this beam preparation can be up to 100%, and is about 40% in the present setup. The additional GVD accrued by the pulses up to the sample, mainly due to the microscope objective (Leica 1.2NA water immersion), is equivalent to a length $L_{MO}=2\text{ cm}$ of SF57 glass. Choosing $L_1=8\text{ mm}$, the linear chirp of Stokes and Pump is equal, so that a constant IFD is achieved. The effect of higher-order dispersion on the IFD matching is discussed in Ref. 14, and creates for the present case an IFD variation of $0.5\text{--}10\text{ cm}^{-1}$ over the pulse duration, depending on t_0 . The Pump pulse is chirped to a duration (intensity full width at half maximum) of $\sim 1\text{ ps}$, corresponding to a Fourier limit of the spectral resolution of the vibrational excitation¹⁴ of 21 cm^{-1} , larger than, and thus not limited by, the higher order effects. The CARS created in the sample is collected by a microscope objective, transmitted through a bandpass filter (triple stack of Omega XF3081, 615–695 nm), and detected by a photomultiplier (Hamamatsu H7422–40).

To demonstrate experimentally the spectral resolution and range accessible with this excitation, we measured CARS from polystyrene (PS) beads of $3\text{ }\mu\text{m}$ diameter, immersed in a gel of 2% agarose and 98% water. CARS images of a cross section through the center of a bead are shown in the insets of Fig. 2. CARS spectra indicated in Fig. 2(a) were obtained from line-scans across the bead as function of t_0 , to measure both the nonresonant CARS from the gel and the CARS from PS. The nonresonant CARS shows the spectral range over which the IFD is tuneable by the delay, centered around 1600 cm^{-1} , and covering roughly the region $1000\text{--}2000\text{ cm}^{-1}$. This range can be extended to the $2700\text{--}3100\text{ cm}^{-1}$ CH region by using a spectrally broader laser source, which is commercially available. In the CARS from PS, several features are visible at spectral positions corresponding to the Raman resonances¹⁵ of PS.

In order to retrieve the CARS spectrum, corrected by the changing temporal overlap between Pump and Stokes, we evaluated the ratio between CARS on PS and the nonresonant CARS in the gel, given in Fig. 2(b). Most of the vibrational resonances show a dispersive shape in the CARS ratio due to the interference with a dominant nonresonant CARS contribution of PS. Moreover, the observed CARS ratio is increasing with decreasing t_0 (and IFD), even though the related Raman intensities (proportional to the imaginary part

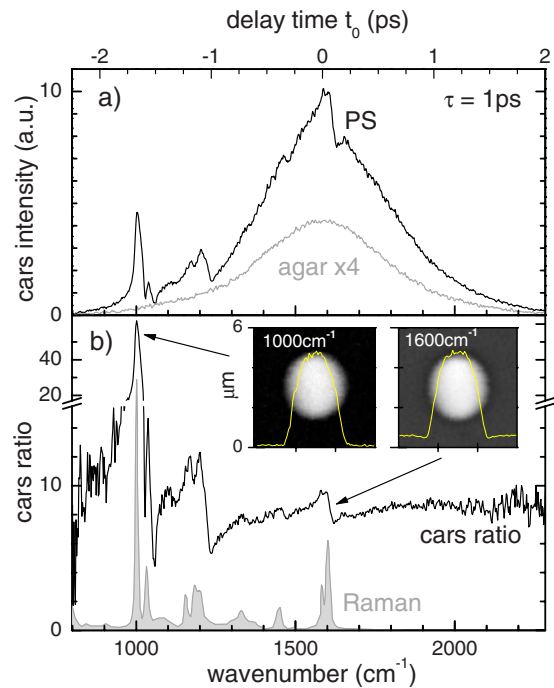


FIG. 2. (Color online) (a) Measured CARS in PS (black) and agar (gray) as function of the delay t_0 . (b) CARS ratio determined from (a) and spontaneous Raman spectrum (Ref. 15) of PS. The images are lateral sections of the $3\text{ }\mu\text{m}$ PS bead for IFDs as labeled. Linear gray scale from zero (black). 61×61 pixels at 0.1 ms/pixel . The yellow lines are horizontal cuts through the bead center. Pump power 7 mW, Stokes power 8 mW.

of the CARS susceptibility) are not showing such a trend. This effect is strongest for the 1001 cm^{-1} resonance (out-of-plane CH deformation), which is dominating the PS nonresonant background by a factor of 8. Such a behavior is expected in spectral focusing CARS due to the time ordering of Pump and Stokes, which is increasing the ratio of resonant to nonresonant contributions with decreasing t_0 , i.e., for a Pump pulse arriving after the Stokes pulse [see Fig. 5a in Ref. 14]. The CARS images of the PS beads [see Fig. 2(b)] taken at 1000 cm^{-1} thus show a better contrast than at 1600 cm^{-1} .

We have recently developed a differential CARS (D-CARS) method,¹⁶ which is a dual-frequency extension of spectral focusing. In short, the Stokes–Pump pulse pair is split into two pairs, the second pair is delayed by half the laser repetition period, and recombined with the first pair. By adding a SF57 glass block of length d to the path of the second pair, its IFD (IFD_2) is reduced compared to the one of the first pair (IFD_1) by the temporal delay introduced between Pump and Stokes due to their different group velocities. The difference of the CARS signals from the two pulse pairs is measured using the ac component of the photomultiplier current filtered by a lock-in (SRS 844) at the laser repetition rate. We also simultaneously acquire the dc component giving the sum of the CARS signals. This method eliminates the spectrally constant nonresonant CARS background and improves the CARS image contrast and chemical sensitivity. We have added to the setup in Fig. 1 the D-CARS pulse duplication unit described in Ref. 16. Transmission through polarizing beam splitters in this unit adds 20 mm of SF2 glass, which increases the linear chirp yielding a pulse duration of 1.3 ps, and we use $L_1=12\text{ mm}$ to match the linear chirp of Pump and Stokes. The resulting Fourier-limited spectral resolution is 16 cm^{-1} .

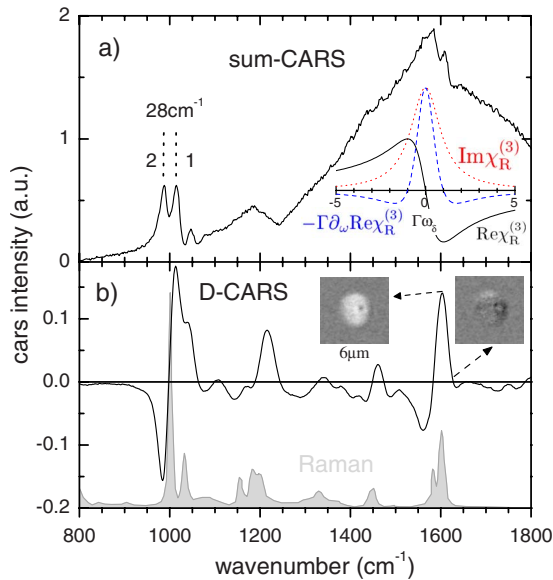


FIG. 3. (Color online) (a) Sum-CARS intensity from a PS bead versus $(IFD_1-IFD_2)/2$. The difference IFD_1-IFD_2 is indicated by vertical lines. Inset: CARS resonant line-shapes (see text). (b) D-CARS corresponding to (a). Bead cross-sections are shown at 1600 cm^{-1} (left) and 1623 cm^{-1} (right) on a gray scale from -0.07 (black) to 0.14 (white). Other conditions as in Fig. 2.

When the resonant CARS contribution is smaller than the nonresonant background, which is for example the case for small concentrations in solution, the CARS lineshape is dominated by the interference $2\chi_{NR}^{(3)}\text{Re}\chi_R^{(3)}$ of the resonant third-order susceptibility $\chi_R^{(3)}=R/(-\omega_\delta-i\Gamma)$ with the nonresonant one $\chi_{NR}^{(3)}$. Here ω_δ is the difference between vibrational excitation and resonance frequency,¹⁴ and Γ is the vibrational dephasing rate. This creates a dispersive lineshape $\text{Re}\chi_R^{(3)}=-R\omega_\delta/(\omega_\delta^2+\Gamma^2)$ [see inset Fig. 3(a)], which is spectrally extended with tails $\propto\omega_\delta^{-1}$. Hence single-frequency CARS is less suited to create specific vibrational contrast than spontaneous Raman, which has a lineshape proportional to $\text{Im}\chi_R^{(3)}=R\Gamma/(\omega_\delta^2+\Gamma^2)$. The spectral differential $\partial_{\omega_\delta}\text{Re}\chi_R^{(3)}=R(\omega_\delta^2-\Gamma^2)/(\omega_\delta^2+\Gamma^2)^2$ however has a shape similar to spontaneous Raman, and even features half the linewidth. By measuring the difference of CARS between two close lying IFDs, we can thus recover a spectral response of high specificity, similar to stimulated Raman scattering.¹⁷ This difference is measured by D-CARS when using a small thickness $d=1\text{ mm}$, resulting in $IFD_1-IFD_2=28\text{ cm}^{-1}$, comparable to the spectral resolution and the relevant Raman linewidths. The corresponding sum-CARS on PS beads [see Fig. 3(a)] shows a duplication of the peaks due to the pres-

ence of the two IFDs (compare with Fig. 2). The D-CARS [see Fig. 3(b)], corrected to represent relative pulse pair intensities resulting in a balanced nonresonant CARS, shows the expected peaked lineshape for the weaker Raman resonances. Cross-section images at 1600 and 23 cm^{-1} off-resonance show the selectivity and the suppression of the nonresonant background in D-CARS. For strong resonances dominating the nonresonant background the D-CARS lineshape becomes dispersive, not suited for good specificity. In this case single CARS can be used, which is available from the measured sum and D-CARS.

In conclusion, we have demonstrated single-frequency CARS microspectroscopy using a single femtosecond laser and passive optical elements which are stable and easy to align. This method offers a spectral resolution comparable to CARS with picosecond sources, as well as fast and broadband spectral tunability, and compatibility with femtosecond-laser techniques such as SHG or TPF. With the dual frequency extension D-CARS,¹⁶ the nonresonant background can be suppressed and the spectral selectivity can be equivalent to Raman or stimulated Raman scattering microscopy.

This work was funded by the U.K. Biotechnology and Biological Research Council (Grant No. BB/D001013/1).

¹A. Zumbusch, G. R. Holtom, and X. S. Xie, *Phys. Rev. Lett.* **82**, 4142 (1999).

²J.-X. Cheng and X. Xie, *J. Phys. Chem. B* **108**, 827 (2004).

³M. Muller and A. Zumbusch, *ChemPhysChem* **8**, 2156 (2007).

⁴A. Volkmer, *J. Phys. D* **38**, R59 (2005).

⁵C. L. Evans and X. S. Xie, *Annu. Rev. Anal. Chem.* **1**, 883 (2008).

⁶J.-X. Cheng, A. Volkmer, L. D. Book, and X. S. Xie, *J. Phys. Chem. B* **105**, 1277 (2001).

⁷J.-X. Cheng, A. Volkmer, L. Book, and X. Xie, *J. Phys. Chem. B* **106**, 8493 (2002).

⁸T. W. Kee and M. T. Cicerone, *Opt. Lett.* **29**, 2701 (2004).

⁹B. von Vacano and M. Motzkus, *Phys. Chem. Chem. Phys.* **10**, 681 (2008).

¹⁰A. S. Weling, B. B. Hu, N. M. Froberg, and D. H. Auston, *Appl. Phys. Lett.* **64**, 137 (1994).

¹¹T. Hellerer, A. M. Enejder, and A. Zumbusch, *Appl. Phys. Lett.* **85**, 25 (2004).

¹²I. Rocha-Mendoza, W. Langbein, and P. Borri, *Appl. Phys. Lett.* **93**, 201103 (2008).

¹³A. F. Pegoraro, A. Ridsdale, D. J. Moffatt, Y. Jia, J. P. Pezacki, and A. Stolow, *Opt. Express* **17**, 2984 (2009).

¹⁴W. Langbein, I. Rocha-Mendoza, and P. Borri, *J. Raman Spectrosc.* **40**, 800 (2009).

¹⁵Polystyrene Raman spectrum <http://www.sigmaaldrich.com/>.

¹⁶I. Rocha-Mendoza, W. Langbein, P. Watson, and P. Borri, *Opt. Lett.* **34**, 2258 (2009).

¹⁷C. W. Freudiger, W. Min, B. G. Saar, S. Lu, G. R. Holtom, C. He, J. C. Tsai, J. X. Kang, and X. S. Xie, *Science* **322**, 1857 (2008).